Slow Dielectric Relaxation of *cis*-Polyisoprene near the Glass Transition Temperature

Keiichiro Adachi* and Hitotsugu Hirano

Department of Macromolecular Science, Graduate School of Science, Osaka University, Toyonaka, Osaka 560, Japan

Received May 14, 1997; Revised Manuscript Received September 12, 1997

ABSTRACT: Dielectric measurements were carried out on undiluted *cis*-polyisoprene (PI) over a wide frequency range from 10^{-4} to 10^5 Hz around the glass transition temperature T_g (=200 K). The data indicate that the dielectric loss curves including both the normal and segmental mode processes are superposable in the range above 230 K (T_g + 30 K). Below 230 K, the time−temperature superposition is not applicable to the whole loss curve. The ratio of the relaxation times of the normal and segmental modes is constant above 230 K but decreases below 230 K with decreasing temperature.

Introduction

Cis-Polyisoprene (PI) exhibits dielectric normal mode relaxation reflecting the fluctuation of the end-to-end vector and the segmental mode relaxation reflecting local motions.[1−4] The relaxation time τ_n for the normal mode depends strongly on the molecular weight and is much longer than the segmental mode relaxation time τ_s. Since our previous experimental window was limited in the range from 20 Hz to 100 kHz, we used the time−temperature superposition principle to cover a wide frequency range.[2,5] The superposition was successfully made over the regions covering both relaxations. In fact, we observed that the Arrhenius plot of τ_n and that of τ_s are parallel to each other. However, Schonhals and co-workers reported that the τ_n and τ_s of low molecular weight PI and poly(propylene glycol) merge around the glass transition temperatures T_g.[6−8] This indicates that the superposition principle does not hold over the frequency ranges where the segmental and normal modes are observed. In the present study, we aimed to examine the conditions and frequency regions where the superposition principle can be applicable. For this purpose, we required an apparatus for measurements in a low-frequency region and attempted to measure ϵ'' of PI by a modified absorption current method with a rectangular wave instead of the usually employed single steplike voltage. We report the method briefly and then the results of the measurements.

Experimental Section

1. Materials. Samples of *cis*-polyisoprene were prepared by anionic polymerization with *sec*-butyllithium as the initiator. Details of the polymerization and characterization were reported previoualy.[1,2] To minimize the effect of the direct current conduction in low-frequency measurements, impurity ions mainly derived from the initiator were carefully removed by repeated precipitation of the PIs from benzene solution in large amounts of methanol and then dried in a vacuum at 40 °C for 5 days. The characteristics are listed in Table 1.

2. Method. Dielectric constant ϵ' and loss factor ϵ'' in the range from 0.02 to 20 kHz were measured with a transformer bridge (General Radio 1615A). An LCR meter (Hewlett-Packard 4284A) was also used to cover the range from 10 to 200 kHz. The measurements in the range from 10^{-4} to 10 Hz were made by a *rectangular wave method* as follows. A similar method in the audio frequency range was reported by Hayakawa et al.[9]

Table 1. Characteristics of PI Samples

Code	M_w	M_w/M_n
PI-10	9 600	1.08
PI-43	43 000	1.08
PI-86	86 000	1.08

Let us consider a capacitor whose empty capacitance is C_o, and the capacitor is filled with a sample of complex dielectric constant $\epsilon^*(\omega) = \epsilon'(\omega) - i\epsilon''(\omega)$. To this capacitor is applied a rectangular voltage with period 2Δ and amplitude V_o (see Figure 1A). The voltage is decomposed into a Fourier series:

$$V^*(\omega) = \frac{2V_o}{\pi}\sum_{p=1}^{\infty}\frac{1}{2p-1}\exp(i\omega_p t) \tag{1}$$

$$\omega_p = \frac{(2p-1)\pi}{\Delta} \tag{2}$$

where i is the unit imaginary number; ω_p is the angular frequency for the $(2p-1)$th harmonics. Theoretically, the summation of eq 1 can be taken up to $p = \infty$, but experimentally, the limiting p is finite due to the finite rising time of the pulse. Then the imaginary current $I^*(\omega)$ is given by

$$I^* = i\omega C_o\epsilon^* V^* \tag{3}$$

From eqs 1 and 3, ϵ' and ϵ'' are given by

$$\epsilon'(\omega_p) = \frac{1}{2V_oC_o}\int_0^{\Delta} I(t)\cos(\omega_p t)\,dt \tag{4}$$

$$\epsilon''(\omega_p) = \frac{1}{2V_oC_o}\int_0^{\Delta} I(t)\sin(\omega_p t)\,dt \tag{5}$$

Here it is noted that the current $I(t)$ is due to the orientational polarization of permanent dipoles, and hence the high-frequency dielectric constant due to electronic polarization is not included in $\epsilon'(\omega_p)$ of eq 4. These equations indicate that if the time dependence of $I(t)$ from time 0 to Δ is measured, the complex dielectric constant at ω_p can be determined.

Figure 1B shows the block diagram of the rectangular wave method. A rectangular wave with an amplitude of 90 V was generated by driving a relay with a pulse generator (Hokuto-denko, HB-104). Two dry batteries supplied positive and negative 90 V, which were stable within 0.1 V. The capacitance cell with the empty capacitance of 130 pF was reported previously.[10] Current was measured with a current amplifier (Keithley, Model 427). When the voltage was changed step-

S0024-9297(97)00678-5 CCC: $15.00
Published on Web 05/19/1998

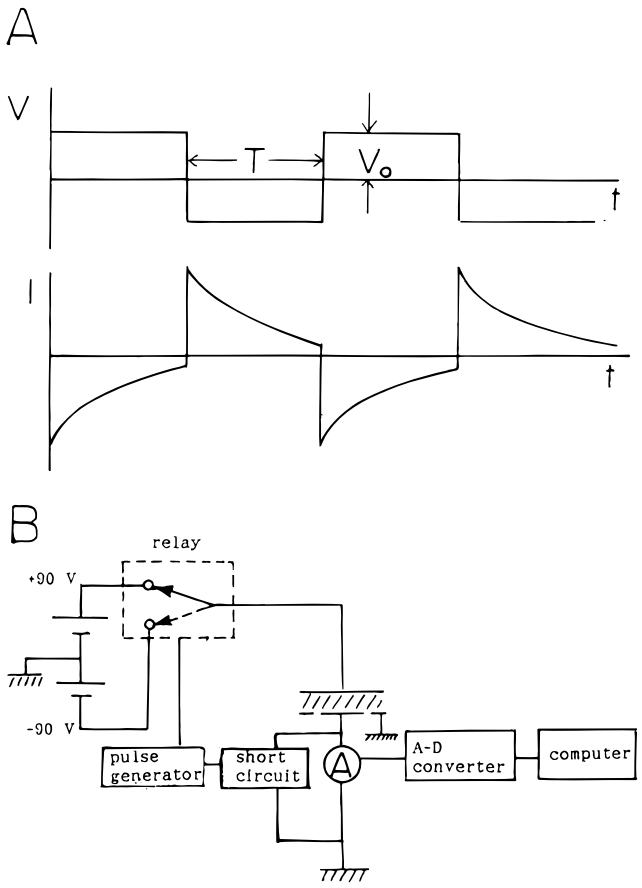

Figure 1. Block diagram of the circuit for measurements of low-frequency dielectric constant and loss.

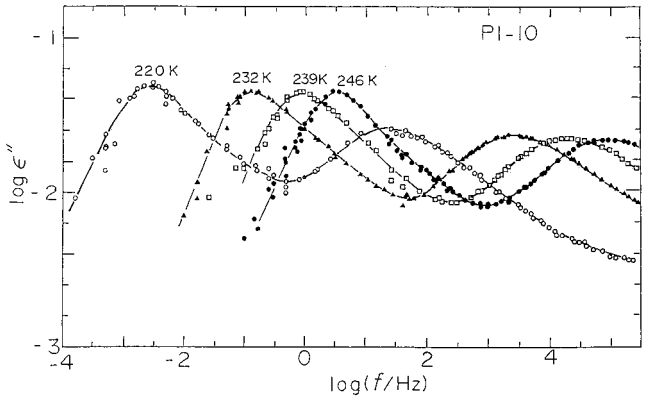

Figure 2. Double logarithmic plots of dielectric loss factor ϵ'' versus frequency f for PI-10. The data points above 20 Hz were obtained by using a bridge and below 20 Hz by the apparatus shown in Figure 1.

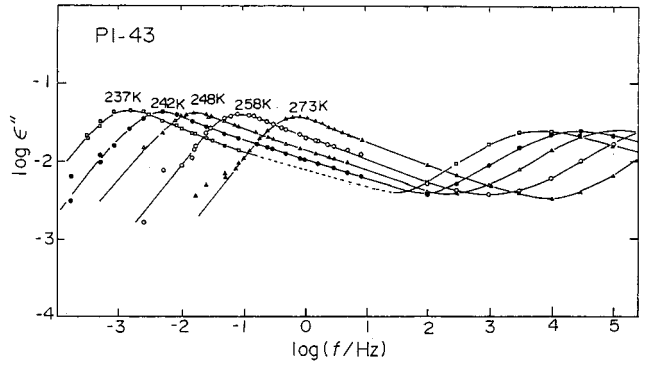

Figure 3. Double logarithmic plots of dielectric loss factor ϵ'' versus frequency f for PI-43. The data points above 20 Hz were obtained by using a bridge and below 20 Hz by the apparatus shown in Figure 1.

wise at time $t = t_1$, an instantaneous large current flowed due to the discharge of the electronic polarization. This current overcame the signal of the orientational polarization for ca. 3 s from t_1. To minimize this effect, we used a gate that short-circuits the electrode and ground for 5 ms from $t = t_1$ to $t_1 +$ 5 ms, as shown in Figure 1.

The output signals from the ammeter were transformed into digital signals and were accumulated in a personal computer (NEC, PC9801). In the measurements at $\Delta < 100$ s, the current was measured for a period of 100 half-waves and the average of the waves was used for the Fourier transform to increase the S/N ratio. For measurements at $\Delta > 100$ s, the measurements were performed for 3 h. The ammeter was calibrated with a circuit composed of a calibrated battery and resistances. Equation 5 indicates that $\epsilon''(\omega_p)$ can be calculated up to infinite frequency. Due to the operation of the short-circuit for the initial 5 ms, $\epsilon''(\omega_p)$ was determined for the modes of $p < 9$. The accuracy of the ϵ' and ϵ'' measurements is estimated to be $\pm 3 \times 10^{-3}$.

Results and Discussion

Dielectric Loss Factor. Figures 2 and 3 show the double logarithmic plot of ϵ'' versus frequency f for PI-10 and PI-43, respectively. The data above 20 Hz were obtained by the bridge method and below 10 Hz by the rectangular wave method. It is seen that the data points obtained by both methods around 10 Hz coincide, indicating the reliability of the rectangular wave method. As reported previously,[1−4] the low- and high-frequency peaks are assigned to the normal mode and segmental mode relaxations, respectively. Since the characteristic molecular weight M_c is 10 000 for PI, PI-43 is in the entangled regime while PI-10 is in the crossover region between the nonentangled regime and the entangled regime. Irrespective of the entanglement effect, the ϵ'' curves thus obtained at temperatures near the glass transition temperature T_g (=200 K) have a shape very similar to the master curves obtained by using the time−temperature superposition principle reported previously.[1−4] This fact indicates that the error of using the time−temperature superposition is small if any.

Applicability of Superposition Principle. To examine the temperature dependence of the distribution of relaxation times, the curves shown in Figures 2 and 3 are superposed by shifting them both in the directions of the abscissa and ordinate. The normalized ϵ'' curves of PI-10 and PI-43 covering both the normal and segmental mode regions are shown in Figure 4A,B, respectively, in which the subscripts n and m represent the normal mode and the loss maximum. For PI-10 the ϵ'' curves measured at temperatures above 232 K are approximately superposable but the curve at 220 K (solid line) is not superposable with the others. Comparing the curve at 220 and those above 232 K, we see that the separation of the loss maximum frequencies between the normal and segmental modes decreases slightly at 220 K. This phenomenon was first reported by Schonhals and co-workers and will be discussed in the next section.[6−8]

For PI-43, we see that the superposition principle holds well. All data shown in Figure 3 are obtained at temperatures above 230 K, and hence the result is consistent with that for PI-10. Thus we conclude that all ϵ'' curves at temperatures above $T_g + 30$ K are superposable. We have reported the shift factor for bulk

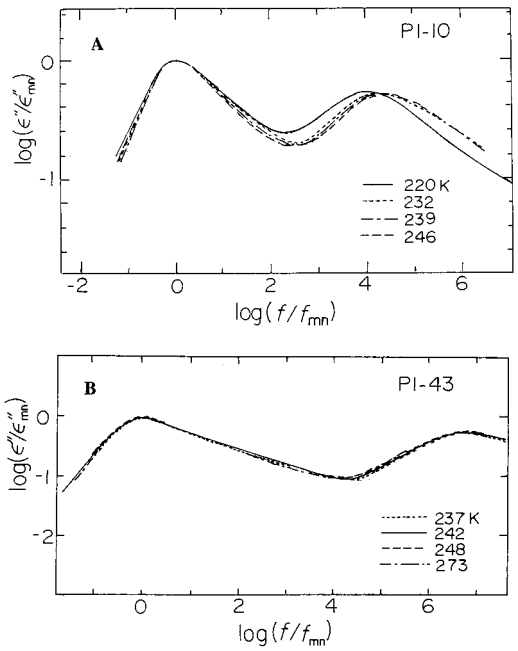

Figure 4. Double logarithmic plot of the normalized ϵ'' curves for (A) PI-10 and (B) for PI-43.

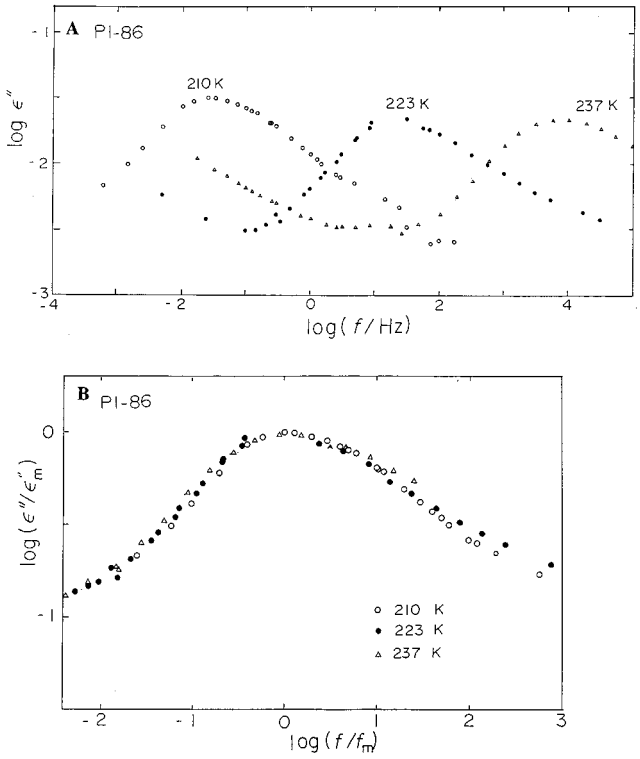

Figure 5. (A) Double logarithmic plot of ϵ'' versus f for PI-86 in the segmental mode region near T_g. (B) Superposition of the data shown in (A).

PIs in the range of temperature above $T_g + 25$ K.[2] The shift factors for the present samples agree with those reported previously.

Figure 5A shows the ϵ'' curves for the segmental mode of PI-86 measured near T_g. The increase of ϵ'' in the low-frequency region of the curves at 223 and 237 K is due to the normal mode relaxation. It appears that the ϵ'' curves narrow slightly with decreasing temperature. However, as shown in Figure 5B, the curves are approximately superposable. This behavior is different from the dielectric behavior observed for many amorphous polymers[11] such as poly(ethyl methacrylate)[12] and poly(vinyl acetate),[13,14] which exhibited broadening of the loss curve with decreasing temperature.

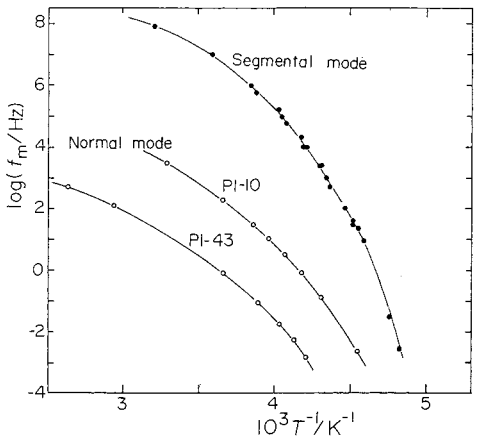

Figure 6. Loss maximum frequency f_m for the normal and segmental modes plotted against $1/T$.

Temperature Dependence of Relaxation Strength. In the above section we have seen that although the whole ϵ'' curve becomes not superposable below 230 K, each of the normal and segmental modes is still superposable near the T_g. In other words, the distribution of relaxation time for the each mode does not change with temperature. In this case, the relaxation strength $\Delta\epsilon$ is proportional to the maximum value of ϵ'' denoted as ϵ''_{max}. Examining the temperature (T) dependence of ϵ''_{max} in Figures 2, 3, and 5, we see that $\Delta\epsilon$ for the normal mode and that for the segmental mode both increase slightly with decreasing temperature. These weak temperature dependences in $\Delta\epsilon$ are due to the density change and the $1/T$ dependence of $\Delta\epsilon$, and hence, both the components of the dipole moment aligned parallel and perpendicular to the chain contour are independent of T within the experimental error.

Temperature Dependence of Relaxation Time. Figure 6 shows the Arrhenius plots of the loss maximum frequencies f_{mn} and f_{ms} for the normal (subscript n) and segmental modes (s), respectively. The ambiguity in the determination of log f_m is ca. ± 0.05 decade throughout this experiment. We see that f_{ms} of PI-10, PI-43, and PI-86 coincide and hence f_{ms} is independent of molecular weight. It is also seen that the ratio of f_{mn} and f_{ms} is almost independent of temperature. Hereafter we call such a behavior "parallel". However, as shown in Figure 7, the ratio of f_{ms}/f_{mn} decreases slightly in the temperature range below ca. 230 K, as pointed out in the previous section. In the range $T > 230$ K, the ratio is almost constant within experimental errors. Recently, Schonhals reported that the ratio has a maximum at a temperature near T_g for poly(propylene oxide).[8] It is difficult to conclude whether this trend is seen in the present data due to the error.

The nominal relaxation time for the normal mode (τ_n) and that for the segmental mode (τ_s) are defined by

$$\tau_j = 1/(2\pi f_{mj}) \tag{6}$$

where j is either n (normal mode) or s (segmental mode). The relaxation time for large scale motions of a macromolecule in the bulk state is given by a form[5]

$$\tau_n = \zeta(T)\, F(M/M_e) \tag{7}$$

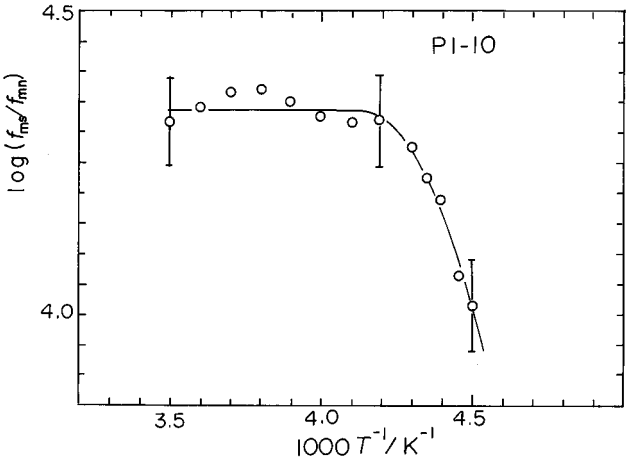

Figure 7. Plot of $\log(f_{ms}/f_{mn})$ versus $1/T$ for PI-10. The error of the values of $\log(f_{ms}/f_{mn})$ is ± 0.1.

where $\zeta(T)$ is the friction coefficient depending on temperature T and $F(M/M_e)$ the structure factor depending on the large scale structure of the macromolecule with the molecular weight M. Here M_e denotes the average molecular weight between entanglements. The parallel change of τ_n and τ_s indicate that $\zeta(T)$ is proportional to τ_s and suggests that the successive segmental motions of a chain result in the large scale motions. In the above section we have seen that τ_n and τ_s are not parallel near T_g. This indicates that at least two shift factors are required to make a composite curve. The shift factor for the normal mode is given by $\zeta(T)/\zeta(T_o)$ at high temperatures since $F(M/M_e)$ is independent of temperature. Here T_o denotes the reference temperature. However, around T_g, $F(M/M_e)$ is expected to depend on temperature, as will be discussed in the final section. We also note that usually the ϵ'' curves for the segmental mode are not superposable near T_g. Therefore, the shift factor cannot be defined in the temperature range near T_g.

For segmental motions, many molecular models have been proposed.[15−22] They are classified into two groups, namely, (1) the theories of local motions in a single chain and (2) those based on the cooperative motions of chains. Among the models of the first group, Helfand[18] proposed a model in which crankshaft-like units rotate around their co-axes under constraints of the barrier for the internal rotation and the viscous drag from the surrounding molecules. The other models based on the single chain implicitly assumed the Kramers model,[23] which expresses the rate of the local conformational change in terms of the barrier for the internal rotation and the local viscous drag from the medium. The local viscosity is different from the macroscopic one, as demonstrated experimentally by Ediger and co-workers.[24] On the other hand, the theories of the second group assume that the barrier height for reorientation of segments depends on the size of the cooperative motional unit. The segmental motion in bulk polymers near T_g was discussed by Matsuoka and Quan[15] and Adachi[16] who proposed the cooperative rearrangement of the segments. These models indicate the distribution of relaxation times of the segmental motion increases with decreasing temperature, especially around T_g. The present results are not in harmony with the theories.

These theories predict little about the relationship between the large scale motion and the local motion. Schonhals[6,7] explained the change of f_{ms}/f_{mn} by considering that τ_s increases with decreasing temperature at the rate higher than τ_n due to the cooperativity of the segmental motions.

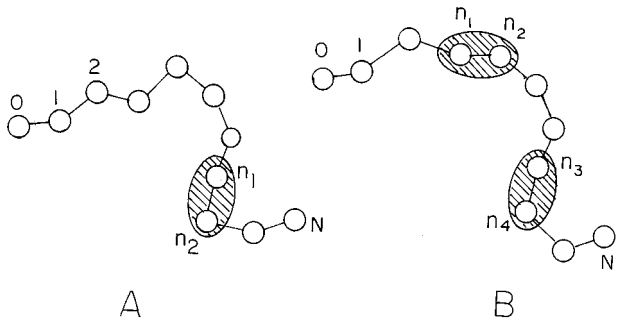

Figure 8. Local vitrification model: (A) Relatively high temperature above T_g and only one part of the chain vitrified; (B) Two parts vitrified with decreasing temperature.

In our previous paper[25] we reported the concentration dependence of τ_n/τ_s for concentrated solutions of PI in toluene: τ_n/τ_s decreases with decreasing concentration. We explained the result by assuming that the size of the unit of local jump increases with decreasing concentration. The molecular weight for the unit of local jump was estimated on the basis of the results of the computer simulation reported by Verdier and Stockmayer.[26] The relationship between the present temperature dependence of τ_n/τ_s near T_g and previous solution data is not clear at the present stage. If we assume that the size of the unit of local jump increases with decreasing temperature due to the cooperativity of the segmental motion, the present result can be consistent with the solution data.

An anonymous reviewer[27] of the present paper suggested an interesting model for the present case, assuming that there exist vitrified regions near T_g, as shown in Figure 8A. The hatched region indicates a local vitrified region. It is expected that the higher normal modes might be more susceptible to local freezing of the molecules as T_g is approached. We assume a chain composed of $N + 1$ beads and, in the hatched region, there are beads with indices n_1 to n_2. Since PI-10 for which the temperature dependence of τ_n/τ_s was observed has a molecular weight close to the characteristic molecular weight, we assume the Rouse model.[28] Then the normal mode relaxation time τ_n is proportional to N^2 before the occurrence of local vitrification but, upon vitrification (Figure 8A), τ_n becomes proportional to the weighted average of $4n_1^2$ and $4(N - n_2)^2$. As T_g is approached, the number of vitrified regions increases, as shown in Figure 8B. Then the beads between the two vitrified parts (from n_1 to n_4) do not contribute to the normal mode relaxation as the vector connecting n_1 and n_4 is fixed. Thus, only the chain ends become dielectrically active. As a result, the apparent relaxation time becomes short and τ_n/τ_s ($=f_{ms}/f_{mn}$) decreases.

However, we expect that local vitrification causes a decrease of the relaxation strength $\Delta\epsilon$ and broadening of the distribution of normal mode relaxation times. Those effects are not seen in the present data: in Figure 4, the distribution of relaxation times is independent of temperature and the dipole moment does not decrease with decreasing temperature. Probably our experiment was conducted ca. 20 deg above T_g and hence the fraction of the vitrified region is still small.

Conclusion

The shape of the ϵ'' curve for the normal mode and that for the segmental mode are independent of temperature. The whole ϵ'' curve covering normal and segmental modes is not superposable below 230K. The ratio τ_n/τ_s decreases with decreasing temperature below 230 K.

References and Notes

(1) Adachi, K.; Kotaka, T. *Macromolecules* **1985**, *18*, 466.
(2) Imanishi, Y.; Adachi, K.; Kotaka, T. *J. Chem. Phys.* **1988**, *89*, 7593.
(3) Adachi, K.; Kotaka, T. *Prog. Polym. Sci.* **1993**, *18*, 585.
(4) Boese, D.; Kremer, F. *Macromolecules* **1990**, *23*, 829.
(5) Ferry, J. D. *Viscoelastic Properties of Polymers*, 3rd ed.; Wiley: New York, 1980.
(6) Schonhals, A.; Kremer, F.; Schlosser, E. *Phys. Rev. Lett.* **1991**, *67*, 999.
(7) Schonhals, A. In *Keynote Lectures in Selected Topics of Polymer Science*; Riande, E., Ed.; Consejo Superior de Investigaciones Cientificas: Madrid, 1995; Chapter 2.
(8) Schonhals, A. *Dielectric Spectroscopy of Polymeric Materials*; Runt, J. P., Fitzgerald, J. J., Eds.; American Chemical Society: Washington, DC, 1997; Chapter 3.
(9) Hayakawa, R.; Kanda, H.; Sakamoto, M.; Wada, Y. *Jpn. J. Appl. Phys.* **1975**, *14*, 2039.
(10) Urakawa, O.; Adachi, K.; Kotaka, T. *Macromolecules* **1993**, *26*, 2042.
(11) McCrum, N. G.; Read, B. E.; Williams, G. *Anelastic and Dielectric Effects in Polymeric Solids*; John Wiley: New York, 1967; Chapters 8−14.
(12) Ishida, Y.; Yamafuji, K. *Kolloid Z.* **1961**, *177*, 97.
(13) Alegria, A.; Guerrica-Echevarria, E.; Goitiandia, L.; Telleria, I.; Colmenero, J. *Macromolecules* **1995**, *28*, 1516.
(14) Nozaki, R.; Mashimo, S. *J. Chem. Phys.* **1987**, *87*, 2271.
(15) Matsuoka, S.; Quan X. *Macromolecules* **1991**, *24*, 2770.
(16) Adachi, K.; *Macromolecules* **1990**, *23*, 1816.
(17) Berry, G. C.; Fox, T. G. *Adv. Polym. Sci.* **1968**, *5*, 261.
(18) Helfand, E. *J. Chem. Phys.* **1971**, *54*, 4651.
(19) Valeur, B.; Jarry, J.-P.; Geny, F.; Monnerie, L. *J. Polym. Sci., Polym. Phys. Ed.* **1975**, *13*, 667.
(20) Hall, K.; Helfand, E. *J. Chem. Phys.* **1982**, *77*, 3275.
(21) Jones, A. A.; Stockmayer, W. H. *J. Polym. Sci., Polym. Phys. Ed.* **1977**, *15*, 847.
(22) Bahar, I.; Erman, B. *Macromolecules* **1987**, *20*, 1368.
(23) Kramers, H. A. *Physica* **1940**, *7*, 284.
(24) Adolf, D. B.; Ediger, M. D.; Kitano, T.; Ito, K. *Macromolecules* **1992**, *25*, 867.
(25) Adachi, K.; Imanishi, Y.; Kotaka, T. *J. Chem. Soc., Faraday Trans. 1* **1989**, *85*, 1083.
(26) Verdier, P. H.; Stockmayer, W. H. *J. Chem. Phys.* **1962**, *36*, 227.
(27) Anonymous reviewer's suggestion.
(28) Rouse, P. E., Jr. *J. Chem. Phys.* **1953**, *21*, 1272.

MA9706788